Statistical physics models for nacre fracture simulation

Phani Kumar V. V. Nukala and Srđan Šimunović
Computer Science and Mathematics Division, Oak Ridge National Laboratory, Oak Ridge, Tennessee 37831-6164, USA
(Received 24 November 2004; revised manuscript received 5 August 2005; published 19 October 2005)

Natural biological materials such as nacre (or mother-of-pearl), exhibit phenomenal fracture strength and toughness properties despite the brittle nature of their constituents. For example, nacre's work of fracture is three orders of magnitude greater than that of a single crystal of its constituent mineral. This study investigates the fracture properties of nacre using a simple discrete lattice model based on continuous damage random thresholds fuse network. The discrete lattice topology of the proposed model is based on nacre's unique brick and mortar microarchitecture, and the mechanical behavior of each of the bonds in the discrete lattice model is governed by the characteristic modular damage evolution of the organic matrix that includes the mineral bridges between the aragonite platelets. The analysis indicates that the excellent fracture properties of nacre are a result of their unique microarchitecture, repeated unfolding of protein molecules (modular damage evolution) in the organic polymer, and the presence of fiber bundle of mineral bridges between the aragonite platelets. The numerical results obtained using this simple discrete lattice model are in excellent agreement with the previously obtained experimental results, such as nacre's stiffness, tensile strength, and work of fracture.

DOI: 10.1103/PhysRevE.72.041919 PACS number(s): 87.68.+z, 62.20.Mk, 46.50.+a

I. INTRODUCTION

Natural biological materials such as shell, bone and dentin are composites of organic proteins and biominerals organized at nanosize length scales. These biological materials exhibit phenomenal fracture strength and toughness properties despite the brittle nature of their constituents. For example, mother-of-pearl, or nacre, is a molluscan shell material that exhibits phenomenal fracture strength and toughness properties despite the brittle nature of its constituents [1–14]. Its work of fracture is about 3000 times greater than that of a single crystal of its constituent mineral [1,2]. This is surprising because it is a ceramic composite made up of about 95% brittle inorganic phase (aragonite, a mineral form of $CaCO_3$) and only a few percent of the soft organic material, and synthetic polymer-matrix composites with such high levels of ceramic fillers do not possess these exceptional combinations of stiffness, fracture strength and toughness. The composite is in the form of a unique "brick and mortar" (BM) microarchitecture with staggered interlaced aragonite platelets bonded together by soft organic layers, wherein the polygonal aragonite platelets represent the bricks and the soft organic material represents the mortar (see Fig. 1). Understanding the mechanisms of such high damage tolerance of nacre will enhance our ability to design materials for innovative practical applications. This understanding is crucial to synthesizing tough ceramics and nanoscale biocomposites that have fracture toughness properties comparable to that of nacre. Research on synthesizing such tough materials is currently under intense development since these materials can be used in various defense related applications including that of light-weight body armour.

In the earlier studies [1,3], nacre's extraordinary fracture properties were believed to be the result of their unique BM microarchitecture. However, synthetic ceramics having the same BM microstructure as that of nacre did not possess fracture toughness characteristics comparable to that of nacre [15]. This led to further investigation of toughening mechanisms that are responsible for nacre's high fracture toughness. Sarikaya *et al.* [5,6] proposed that nacre's high fracture resistance is due to sliding of platelets and formation of organic ligaments between platelets. Wang *et al.* [7] proposed that crack deflection, branching and diversion combined with platelet pullout and organic matrix bridging is the primary mechanism leading to nacre's high toughness. Roughness of the platelet interfaces between the aragonite platelets and the organic matrix has been proposed to be the main toughening mechanism in Refs. [10,11]. Since the synthetic ceramics having the BM microstructure with inorganic matrix binding the platelets did not possess similar toughness values, Almqvist *et al.* [15] suggested that the key to the nacre's high toughness could lie in the organic matrix that binds the aragonite platelets. In particular, Almqvist *et al.* [15] pointed out that ceramic composites with organic interfaces possess higher fracture toughness compared to inorganic interfaces. Subsequently, Smith *et al.* [8] proposed a mechanism based on modular damage evolution of organic polymer adhesive to explain the high fracture toughness of nacre. Okumura *et al.* [12,16] have suggested that stress concentration is significantly reduced by the presence of soft organic matrix and this leads to higher toughness values of nacre. Recently, Schaffer *et al.* [17] and Song *et al.* [18,19] have proposed that the presence of mineral bridges between the aragonite platelets combined with the modular damage evolution of the organic polymer adhesive is the main mechanism leading to phenomenal toughness of nacre. The relative abundance of previous research on the toughening mechanisms of nacre suggests that the main toughening mechanism that leads to nacre's high toughness is yet to be well understood.

The toughening mechanisms of nacre have also been studied using various analytical [20,21] and numerical [22–24] models. Although these analytical and numerical models have been successful in estimating the nacre's stiffness accurately, a good comparison with nacre's (experimental) strength, ductility and toughness values was not achieved. The previous modeling studies have hinted at the possible

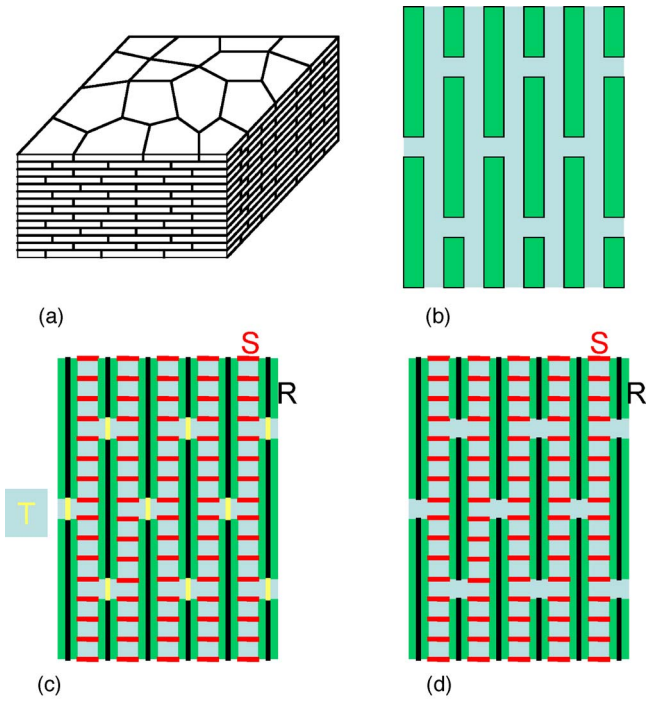

FIG. 1. (Color online) Schematics of (a) Sheet nacre (top left). (b) Brick and mortar (BM) architecture of nacre (top right). (c) Square lattice topology representing the nacre's BM architecture. The matrix shear and tension elements connect, respectively, the long and short edges of the platelets. The aragonite platelets are represented by ρ (aspect ratio) number of mineral tension elements to simulate building up of tensile stresses from the ends of the platelets (bottom left). (d) Square lattice topology without the matrix tension elements that connect the short edges of aragonite platelets (bottom right).

reasons behind nacre's toughness values based on certain indirect measurements and arguments. In this study, we investigate the fracture of nacre using discrete lattice models based on statistical physics methodology. The discrete lattice model proposed in this study captures the essential physics of the problem; namely, the unique BM microarchitecture, crack diversion and braching mechanisms, modular damage evolution of the organic polymer adhesive, and the presence of mineral bridges between the aragonite platelets. The stress concentration effects in the vicinity of crack tips are automatically captured by the numerical model while solving the system of governing equations. The numerical results obtained using this simple discrete lattice model are in excellent agreement with the previously obtained experimental results, such as nacre's stiffness, tensile strength, and work of fracture.

Discrete lattice models have often been used to understand the scaling properties of fracture in disordered materials. A very well studied model is the random fuse model (RFM), where a lattice of fuses with random thresholds are subject to an increasing voltage [25–28]. A resistor network represents a scalar analog of an elastic medium and is thus relatively simple to analyze, while retaining the essential characteristic features of the problem. However, in order to capture the modular damage evolution in the organic interface that binds the aragonite platelets, we use a continuous damage random thresholds fuse model (CDRFM) [29], wherein damage evolves in a modular fashion corresponding to the sawtoothlike force-extension behavior of the organic matrix that bonds aragonite platelets (see Fig. 2). A similar model has also been introduced for fiber bundle models in Refs. [30,31]. Indeed, the modular sawtoothlike force-extension behavior of CDRFM is consistent with the force-extension behavior of a fiber bundle of mineral bridges between the aragonite platelets and the force-extension curves corresponding to a repeated unfolding of protein molecules in the organic polymer adhesive. It is in this sense that the multiple failures of fuses in the CDRFM represent the effect of mineral bridges and the organic polymer adhesive. It should be noted that continuous damage spring and beam lattice networks may also be used (see Ref. [32]), however, CDRFM is a simple scalar discrete lattice model with fewer degrees of freedom than the corresponding spring and beam lattice analogs.

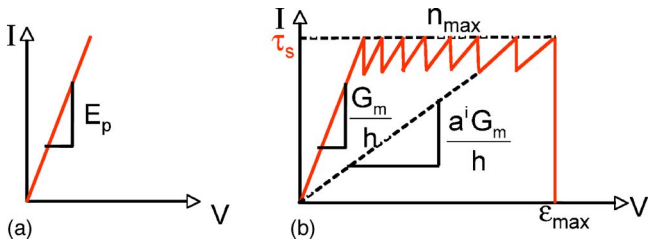

FIG. 2. (Color online) Schematic of (a) mineral tension element (fuse) behavior (left), and (b) matrix shear element (fuse) behavior.

II. MODEL

The unique BM microarchitecture of nacre is modeled by a square lattice network as shown in Fig. 1. The shear elements (fuses), S, connect the long edges of the aragonite platelets and the tension elements (fuses), T, connect the short edges of the aragonite platelets. The aragonite platelets are represented by mineral elements (fuses) denoted by R. The geometric features of the square lattice can be expressed in terms of aragonite platelet dimensions. Assuming the thickness of the platelet to be of unit dimension, the length of the platelet is given by the aspect ratio, ρ, which denotes the ratio of the length of the platelet to the thickness of the platelet. The thickness of the organic matrix is denoted by h, where h denotes the ratio of organic matrix thickness to the thickness of the platelet.

We assume that the aragonite platelets carry tensile stresses and the stress is transferred from one platelet to the other by shear in the organic matrix. We also assume that the tensile stresses change along the length of the platelets and these stresses build up from the ends of the platelet [1]. That is, the tensile stresses at the ends of the platelets is zero, and hence the tension elements, T, do not carry any tensile stresses. This is equivalent to removing the tension elements from the model. In addition, the length dimension of the aragonite platelets is divided into ρ number of R elements in order to represent the building up of tensile stresses in the

platelets. Based on the above observations, the model that we use in the numerical simulations is the model shown in Fig. 1 without the tension elements, T. This is in agreement with the earlier models based on shear lag theory [1,20]. However, the present model incorporates the platelet interaction effects and the redistribution of stresses automatically.

In the traditional random thresholds fuse model (RFM), the lattice is initially fully intact with bonds having the same conductance, but the bond breaking thresholds, t, are randomly distributed based on a thresholds probability distribution, $p(t)$. The burning of a fuse occurs irreversibly, whenever the electrical current in the fuse exceeds the breaking threshold current value, t, of the fuse. In the CDRFM, however, multiple failures of the fuses are allowed depicting the modular damage evolution of the organic matrix. That is, in principle, a fuse representing the organic matrix can fail more than once, and we define $n_{\max}$ as the maximum number of failures allowed for each of the shear (S) elements. Whenever the electrical current in the fuse exceeds the breaking threshold current value, t, of the fuse, the conductance of the fuse is reduced by a factor $a(0<a<1)$. Once a fuse has failed $n_{\max}$ number of times, we allow for brittle failure of the fuse. That is, the fuse is burnt irreversibly after $n_{\max}$ number of failures. The numerical value of $n_{\max}$ is chosen based on the values of maximum strain (potential difference) that the bonds can withstand before failing irreversibly.

Assuming a unit out-of-plane dimension, since the length and thickness of each of the mineral tension elements is also of unit dimension, the conductance of each of the mineral elements (R) is set equal to E_p, where E_p is the Young's modulus of the aragonite platelet. We assume that the ultimate strength of the aragonite platelets is not reached during loading, i.e., the mineral tension elements do not break. The initial conductance of each of the shear elements (S) is set equal to G_m/h, where G_m denotes the initial shear modulus of the organic matrix layer. The bond breaking threshold current at which the shear elements (fuses) break irreversibly is prescribed randomly based on a thresholds distribution $p(t)$. Whenever the current in the shear elements (fuses) exceeds the breaking threshold current value, t, of the fuse, the conductance of the fuse is reduced by a factor $a(0<a<1)$. Consequently, the conductance of the organic matrix layer after $1 \leqslant i \leqslant n_{\max}$ number of breaks is given by G_i/h, where $G_i = a^i G_m$. Once a shear element (fuse) has failed $n_{\max}$ number of times, the fuse is burnt irreversibly. A schematic of mineral and shear element's (fuse) behavior for the CDRFM is presented in Fig. 2. Periodic boundary conditions are imposed in the horizontal direction to simulate an infinite system and a constant voltage difference, V, is applied between the top and the bottom of lattice system bus bars.

Numerically, a unit voltage difference, $V=1$, is set between the bus bars and the Kirchhoff equations are solved to determine the current flowing in each of the fuses. Subsequently, for each fuse j, the ratio between the current i_j and the breaking threshold t_j is evaluated, and the conductance of the bond j_c having the largest value, $\max_j(i_j/t_j)$, is reduced by a factor $a(0<a<1)$. If the fuse j_c fails more than $n_{\max}$ number of times, the fuse j_c is irreversibly removed (burnt), otherwise, the breaking threshold of the fuse j_c is either unchanged (quenched disorder) or a different threshold t is chosen for the fuse j_c based on the probability distribution $p(t)$ (annealed disorder). The current is redistributed instantaneously after the fuse failure implying that the current relaxation in the lattice system is much faster than the failure of a fuse. Each time a fuse fails, it is necessary to recalculate the current redistribution in the lattice to determine the subsequent failure of a fuse. The process of fuse failures, one at a time, is repeated until the lattice system falls apart. This process of failure of one fuse at a time corresponds to the quasistatic approximation. It is well known that simulations based on discrete lattice models (fuse, spring and beam models) often lead to somewhat unphysical I-V (stress-strain) curves due to this quasistatic process of breaking one fuse (bond) at a time [27]. In particular, they correspond neither to a current (stress) controlled nor to a voltage difference (strain) controlled experiment due to the finite stiffness of the loading device and the fact that the current (or stress) relaxation times are much smaller than the time taken by the loading device to react to the fuse failure event. However, the same breaking sequence is expected when the voltage difference (strain control) or the total current (stress control) is increased at an infinitesimal rate [27].

In this work, we consider two scenarios; one in which the thresholds distribution for the shear elements is given by $p(t)=\tau_s$, where τ_s is the mean shear strength of the organic matrix and this scenario corresponds to the case of no disorder in the thresholds, and the other in which the thresholds distribution is given by a uniform probability distribution between $[\tau_s-\Delta, \tau_s+\Delta]$, where 2Δ is the range of the thresholds about the mean value of τ_s. With these features, the proposed numerical model captures the unique features of nacre, namely, the modular damage evolution of the organic polymer adhesive, the modular damage evolution of the fiber bundle of mineral bridges connecting the adjacent aragonite platelets, and the BM microarchitecture.

Numerical simulation of fracture using large fuse networks is often hampered due to the high computational cost associated with solving a new large set of linear equations every time a new lattice bond fails. The authors have developed rank-1 sparse Cholesky factorization updating algorithm for simulating fracture using discrete lattice systems [33]. In comparison with the Fourier accelerated iterative schemes [34] used for modeling lattice breakdown, this algorithm significantly reduced the computational time required for solving large lattice systems.

III. NUMERICAL SIMULATIONS

For the numerical simulations, we employ a $L \times L$ square fuse lattice network with periodic boundary conditions in the horizontal direction and a constant voltage difference V is applied between the top and bottom bus bars. As representative values, we assume the following geometric and material properties [3,4,18,19]: the thickness of the aragonite platelet is assumed to be 500 nm [14,18,19] and corresponds to a unit dimension, the platelet aspect ratio is assumed to be $\rho = 8$ [3,4,19] corresponding to a length of 4 μm [18,19], and the thickness of the organic layer is assumed to be 25 nm

[19] resulting in a nondimensional value of $h=\frac{1}{20}$. A perfect sheet nacre BM arrangement of platelets is represented by a platelet overlap of $\rho_{\text{olap}}=50\%$. For the purposes of 2D numerical simulation, the width of the platelet in the out-of-plane direction is assumed to be of unit dimension. The Young's modulus of the aragonite mineral and the shear modulus of the organic matrix are assumed to be $E_p=100$ GPa [4] and $G_m=4.6$ GPa [4,19], respectively.

In the fuse lattice network analogy, the conductances of the mineral tension elements (R), correspond to the axial stiffnesses of the elastic spring elements, and are equal to E_p since the thickness and length of each mineral tension element is of unit dimension. Similarly, the initial conductances of the shear elements (S), correspond to the shear stiffnesses of elastic shear springs, and are equal to G_m/h. Before proceeding with the statistical properties of nacre fracture, we perform a deterministic fracture simulation of nacre using the above representative set of parameters. For this representative set of numerical simulations, we assume that there is no disorder in the bond breaking thresholds. Consequently, the bond breaking thresholds distribution is given by $p(t)=\tau_s$, where we set the mean shear strength of the organic matrix τ_s to be equal to 46 MPa for dry nacre [4,10,11,21]. We assume that the modular damage evolution in the organic layer is represented by multiple failures of shear elements, and we set $a=0.9$ to signify that the conductivity of the fuse drops to 90% of its previous value after every repeated failure of the fuse until the maximum number of failures of the fuse is reached at which time the fuse is broken and the stiffness is reduced to zero. The representative value for the maximum number of failures a fuse can break is set at $n_{\max}=\log(\epsilon_0/\epsilon_{\max})/\log a\approx 50$ corresponding to a maximum shear strain of $\epsilon_{\max}=0.10$ (10%) in the organic matrix [10,11,21], where $\epsilon_0=h\tau_s/G_m$.

In the following, we present the typical numerical results obtained from a fuse lattice system of size $L=64$. The results presented below seem to indicate that the scaling effects associated with lattice system sizes are not significant for this lattice system size of $L=64$. However, wherever appropriate, we compare the numerical results for both systems $L=64$ and $L=128$. Figure 3 presents a typical stress-strain response and its envelope obtained using the CDRFM. As mentioned earlier, the unrealistic nature of stress-strain response (zig-zag curve in Fig. 3) is a manifestation of breaking one bond at a time using any of the discrete lattice models (fuse, spring, and beam models). This fact is well known in the literature (see Ref. [27]; in particular see pp. 172 and 181 of *Damage and Fracture of Disordered Materials*, edited by D. Krajcinovic and J.G.M. van Mier), and is due to the usage of discrete lattice models for simulating fracture of quasibrittle materials. The envelope of this zig-zag stress-strain response however is similar to the experimental response, where tensile failure in materials occurs at constant strain. In general, the zig-zag parts of the stress-strain response are often used to assess the avalanche signal characteristics of fracture process.

In presenting our numerical results, we adopt the following nomenclature. The stiffness refers to the initial slope of the stress-strain curve (I/L versus V/L). The peak current

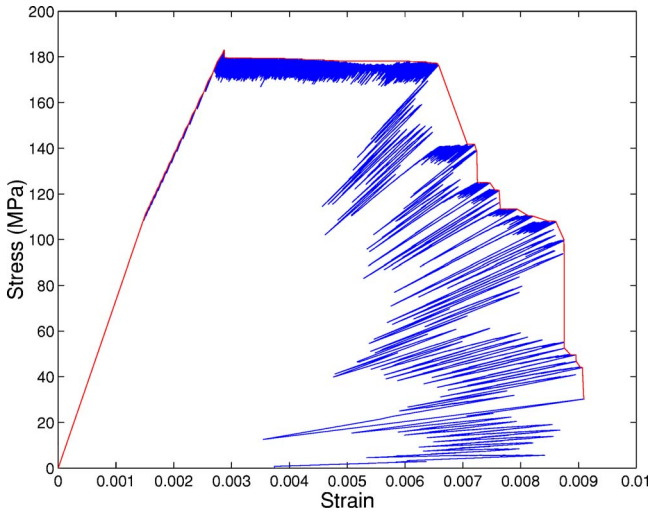

FIG. 3. (Color online) Envelope of a typical stress-strain response obtained using the CDRFM.

$I_{\max}$ in the fuse lattice network corresponds to the peak load $F_{\max}$ of the lattice system. The tensile strength is given by $\sigma_{\max}=F_{\max}/L$. Ductility refers to the ability of the material to plastically deform, and in this sense we refer to the amount of strain in the plateau region of the stress-strain curve as the ductility. The toughness is referred to in the sense of work of fracture, which is defined as the area under the (nominal) stress-strain diagram multiplied by the length of the specimen.

A. Stiffness

Using the above representative material properties, the initial conductance of the fuse lattice network is computed to be 73.61 units, which corresponds to a lattice system stiffness of 73.61 GPa. The computed stiffness is in close agreement with the experimentally determined (dry) nacre stiffness of 70 GPa [4]. It should be noted that besides the Young's modulus E_p of the aragonite mineral and the shear modulus G_m of the organic matrix, there are many other factors such as the ratio of organic layer thickness to the thickness of the aragonite platelet, h, the aspect ratio of the platelet, ρ, and the amount of overlap, ρ_{olap}, of the aragonite platelets (sheet nacre or columnar nacre) that effect nacre's stiffness. Figure 4 presents the variation of nacre stiffness with these (G_m, h, ρ, and ρ_{olap}) parameters. When simulations are performed on a lattice system of size $L=128$, the lattice system stiffness is estimated to be 73.52 GPa. From these results, it is clear that the scaling effects associated with lattice system sizes are negligible on the lattice system stiffness.

Instead of assuming a perfect BM microarchitecture with constant aspect ratios and platelet overlaps (ρ and ρ_{olap}), we have also analyzed a random square lattice network in which the aspect ratio, ρ, of each of the platelets is chosen at random based on a uniform probability distribution such that $\rho\in[6,10]$, while keeping all other parameters ($G_m=4.6$ GPa and $h=\frac{1}{20}$) at their representative values. Figure 5 shows the final crack in a typical lattice sample of size L

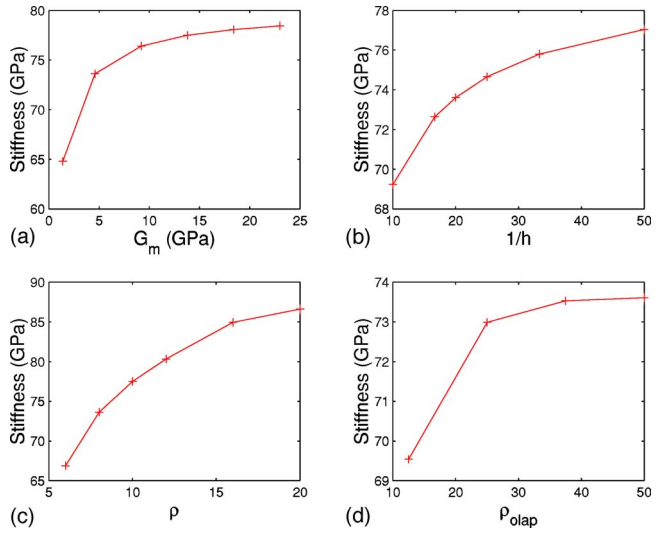

FIG. 4. (Color online) Parametric study of nacre's stiffness for $L=64$. The base line study is for $G_m=4.6$ GPa, $h=\frac{1}{20}$, $\rho=8$, and $\rho_{\text{olap}}=50\%$. (a) Effect of the shear modulus of organic matrix. The stiffness of wet nacre with $G_m=1.4$ GPa is 64.80 GPa. (b) Effect of the ratio of organic layer thickness to the thickness of the platelet. (c) Effect of the platelet aspect ratio. (d) Effect of sheet or columnar microarchitecture of nacre.

$=64$. For $L=128$, the mean stiffness of such a lattice network is estimated to be 74.16 GPa based on 25 sample lattice configurations.

B. Tensile strength

In addition to a constant thresholds value $p(t)=\tau_s$, we have also investigated the tensile strength of a lattice network with bond thresholds randomly prescribed based on an uniform probability distribution between $[\tau_s-\Delta,\tau_s+\Delta]$, where $\tau_s=46$ MPa and $\Delta=6$ MPa. For the representative set of properties ($G_m=4.6$ GPa, $h=\frac{1}{20}$, $\rho=8$, and $\rho_{\text{olap}}=50\%$), the stress-strain response as obtained by the I/L-V/L response of the fuse lattice network is presented in Fig. 6 for both constant and uniform bond thresholds distributions. For the constant bond thresholds value $[p(t)=\tau_s]$, the tensile strength predicted by the fuse lattice network is 182.9 MPa although the plateau of the stress-strain response is approximately at 175 MPa. For the uniform thresholds distribution ($t\sim\text{Uniform}[\tau_s-\Delta,\tau_s+\Delta]$), the mean tensile strength based on 25 sample configurations is 173.3 MPa whereas the plateau of the stress-strain response is slightly below approximately at 170 MPa. The tensile strengths computed by using larger lattice system of size $L=128$ for constant and uniform thresholds distributions are 182.9 MPa and 172.7 MPa, respectively, which are once again in good agreement with the values computed by a lattice network of size $L=64$. It should be noted that the predicted tensile strengths using the fuse lattice network are in excellent agreement with the experimentally measured tensile strength of 167 MPa for dry nacre [4].

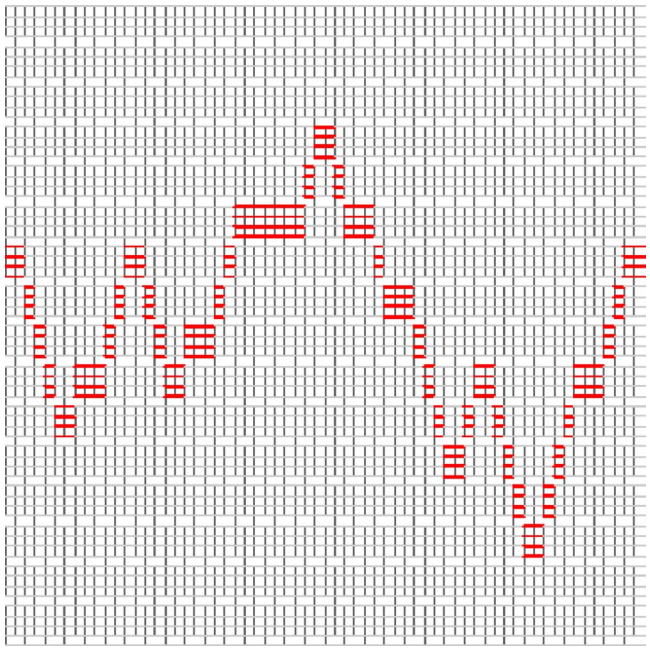

FIG. 5. (Color online) Fractured surface of a typical lattice sample configuration of size $L=64$.

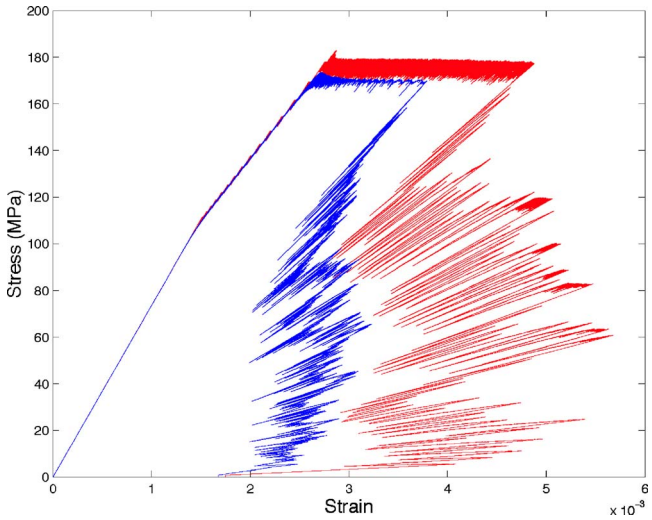

FIG. 6. (Color online) Stress-strain response of nacre. The I-V response of the fuse lattice network is normalized with the lattice system size L to obtain the stress-strain response. The parameters used are $L=64$, $G_m=4.6$ GPa, $\epsilon_{\max}=10\%$, $h=\frac{1}{20}$, $\rho=8$, and $\rho_{\text{olap}}=50\%$. The stress-strain response exhibits a constant plateau indicating significant ductility. Red curve (the one with most ductility) represents the case of constant thresholds value whereas the blue curve (less ductility curve) represents the typical stress-strain response in the case of uniform thresholds distribution.

The effect of sheet and columnar BM microarchitecture on the tensile strength can be investigated by changing the amount of overlap, ρ_{olap}, keeping all other parameters constant. Figure 7 presents the effect of aragonite platelet overlap on the tensile strength of nacre for the representative set of values. The results presented in Fig. 7 indicate that the tensile strength is significantly effected by the amount of platelets overlap. That is, for the same set of parameters, sheet nacre has a higher tensile strength than that of colum-

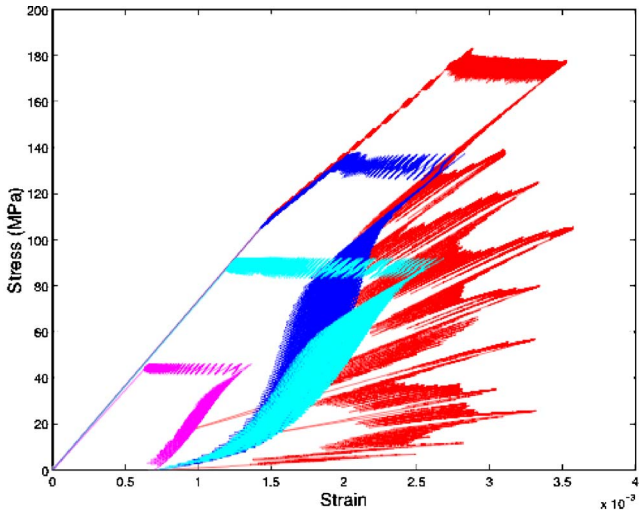

FIG. 7. (Color online) Effect of platelet overlap, ρ_{olap} on the tensile strength of nacre. The parameters used are $L=128$, $G_m=4.6$ GPa, $\epsilon_{\max}=10\%$, $h=\frac{1}{20}$, $\rho=8$, and $n_{\max}=50$. We consider platelet overlaps of $\frac{4}{8}$ [$\rho_{\text{olap}}=50\%$, red (top most)], $\frac{3}{8}$ [$\rho_{\text{olap}}=37.5\%$, blue (second from top)], $\frac{2}{8}$ [$\rho_{\text{olap}}=25\%$, cyan (third from top)], and $\frac{1}{8}$ [$\rho_{\text{olap}}=12.5\%$, magenta (bottom)]. The tensile strength depends significantly on the amount of overlap of platelets.

nar nacre although the stiffness is the same in both cases. In addition to the perfect BM arrangement of platelets, we have also considered the effect of random geometry (ρ and ρ_{olap} are random) on the stress-strain response of nacre. Once again, the results presented in Fig. 8 clearly indicate that the tensile strength of the lattice system is significantly influ-

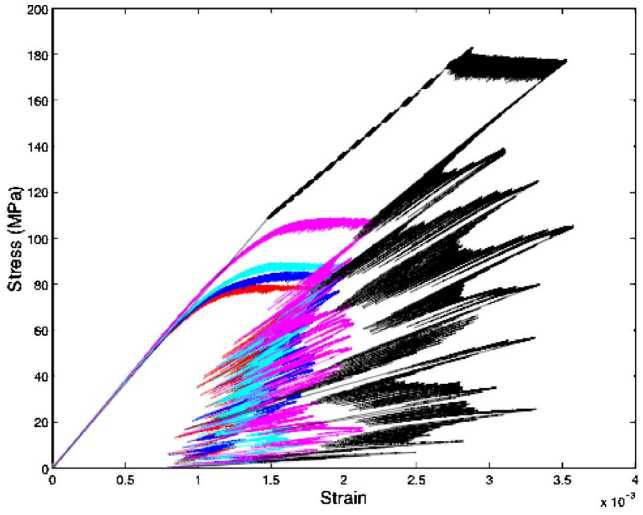

FIG. 8. (Color online) Effect of randomness in the BM arrangement of platelets on the tensile strength of nacre. The randomness in the BM arrangement of platelets is equivalent to random ρ and ρ_{olap} values with ρ uniformly distributed in the range $[8-\delta,\ 8+\delta]$. The reference parameters used are $L=128$, $G_m=4.6$ GPa, $\epsilon_{\max}=10\%$, $h=\frac{1}{20}$, and $n_{\max}=50$. (a) $\delta=4$ (red), (b) $\delta=3$ (blue), (c) $\delta=2$ (cyan), (d) $\delta=1$ (magenta), (e) $\delta=0$ (black), same as $\rho=8$ and $\rho_{\text{olap}}=50\%$ (red) plot of Fig. 7. A perfect BM arrangement of platelets with maximum overlap area (i.e., $\rho_{\text{olap}}=50\%$) significantly increases the tensile strength of nacre.

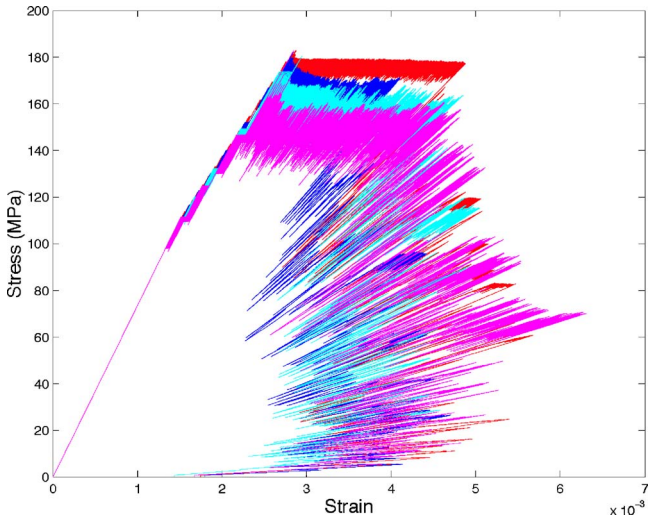

FIG. 9. (Color online) Effect of conductivity reduction factor, a, on the tensile strength of nacre. The parameters used are $L=64$, $G_m=4.6$ GPa, $\epsilon_{\max}=10\%$, $h=\frac{1}{20}$, $\rho=8$, and $\rho_{\text{olap}}=50\%$. We consider the following four values: $a=0.9$ [$n_{\max}=50$, red (top most)], $a=0.8$ [$n_{\max}=24$, blue (second from top)], $a=0.7$ [$n_{\max}=15$, cyan (third from top)], $a=0.6$ [$n_{\max}=11$, magenta (bottom)]. The tensile strength (maximum of stress-strain response) in all of the cases is approximately the same (182.7 MPa, 182.3 MPa, 180.5 MPa, and 183 MPa, respectively), however, smaller a values lead to a large drop in the tensile strength before the response is stabilized.

enced by the randomness of the lattice geometry and the amount over which the platelets overlap. The overall stress-strain response presented in Figs. 6–8 [the stiffness, the stress-strain plateau, and the strain at which plateau (or yielding) sets in] is in excellent agreement with the experimental stress-strain response presented in Fig. 1 of Ref. [10] [or Fig. 5(b) of Ref. [11]]. Based on the results presented in Fig. 8, the lower yield stress in these figures can be explained on the basis of amount of overlap of aragonite platelets of nacre. We have also considered the combined effect of random geometry (ρ and ρ_{olap} are random) and random uniform thresholds distribution on the stress-strain response of nacre. The results indicated that randomness (variation Δ about the mean shear strength τ_s) in the breaking thresholds of the shear elements (organic matrix) did not have as significant of an effect on nacre's tensile strength as the randomness in the platelet aspect ratios and their overlap, although increasing the mean shear strength significantly increases the tensile strength.

As mentioned earlier, multiple failures of shear elements (fuses) represent the modular damage evolution of the organic matrix, which can be attributed to the presence of fiber bundle of mineral bridges between the aragonite platelets and the repeated unfolding of protein molecules in the organic polymer adhesive. In the CDRFM, the conductivity of the fuse elements is reduced by a factor a after each failure of the fuse element until a maximum of $n_{\max}$ times. Figure 9 presents the effect of the reduction factor a on the lattice network stress-strain response. The stress-strain response is qualitatively similar for all of the a values considered in the study.

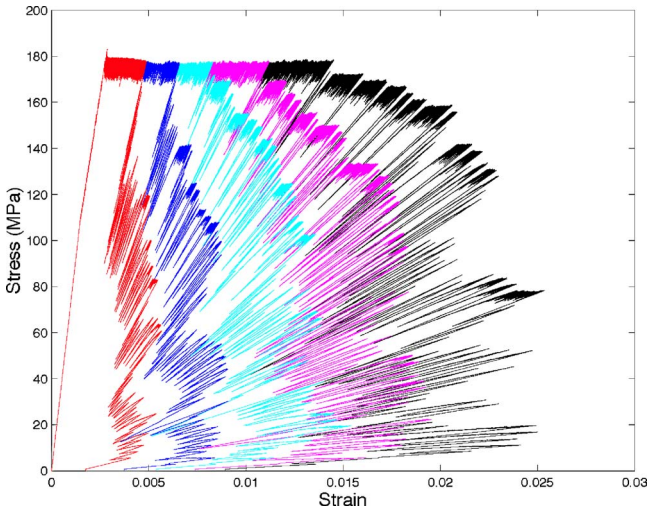

FIG. 10. (Color online) Effect of maximum shear strain, ϵ_{max}, in the organic matrix on the work of fracture of nacre. The parameters used are $L=64$, $G_m=4.6$ GPa, $h=\frac{1}{20}$, $\rho=8$, and $\rho_{olap}=50\%$. We consider maximum shear strains of $\epsilon_{max}=10\%$ (red, minimum ductility), $\epsilon_{max}=20\%$ (blue), $\epsilon_{max}=31\%$, (cyan), $\epsilon_{max}=42\%$, (magenta), and $\epsilon_{max}=52\%$ (black, maximum ductility).

C. Work of fracture

It is clear from Figs. 6 and 7 that the macroscopic response exhibits significant ductility due to the modular damage evolution (multiple failure of fuses) of shear elements. In Figs. 6 and 7, we have limited the maximum shear strain, ϵ_{max}, in the organic matrix to 10%. Figure 10 presents the effect of ϵ_{max} on the work of fracture. The work of fracture increases significantly with the increasing maximum shear strain values in the organic matrix. From the results presented in Fig. 10, it is clear that a macroscopic strain of 1% in the tension experiment corresponds to about 30%–40% shear strain in the organic matrix. Figure 11 presents the stress-strain response when the fibrils are assumed to withstand a maximum strain of 150% [4]. The corresponding macroscopic strain is between 8%–9%. The results presented in Figs. 10 and 11 suggest that the work of fracture of nacre is orders of magnitude larger than that corresponding to aragonite mineral.

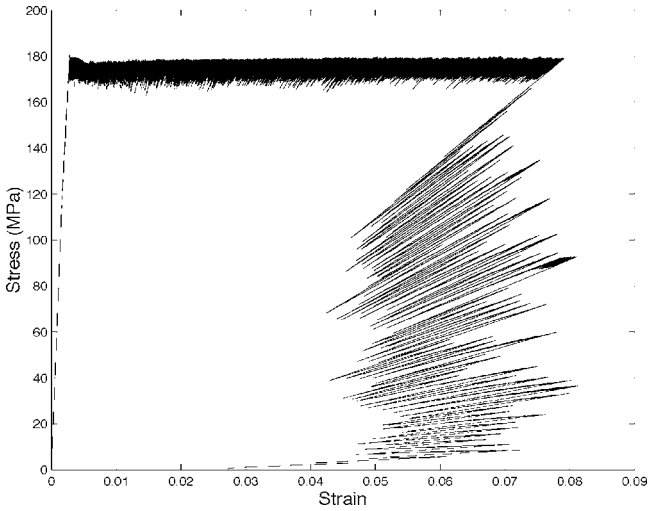

FIG. 11. Stress-strain response when the maximum shear strain in the organic matrix is set to $\epsilon_{max}=150\%$. The parameters used are $L=64$, $G_m=4.6$ GPa, $h=\frac{1}{20}$, $\rho=8$, and $\rho_{olap}=50\%$.

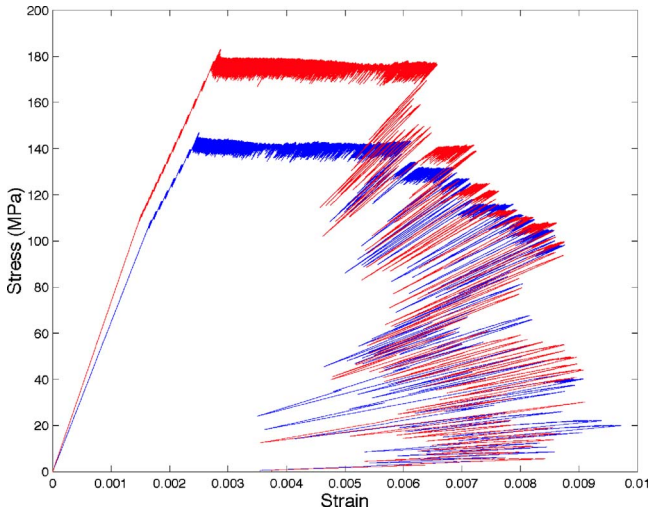

FIG. 12. (Color online) Comparison of wet and dry nacre stress-strain response. The parameters used are $L=64$, $\epsilon_{max}=20\%$, $h=\frac{1}{20}$, $\rho=8$, and $\rho_{olap}=50\%$. Red curve (top curve) represents the dry nacre response whereas the blue curve (bottom curve) represents the wet nacre response.

D. Wet nacre

In general, the effect of water is to decrease the shear modulus of the organic matrix and increase its ductility. The shear modulus of the organic matrix of wet nacre is assumed to be $G_m=1.4$ GPa [4]. Consequently, the initial conductances of the shear elements is set to $1.4\times 20=28$ units. For wet nacre, the mean shear strength of the organic matrix is assumed to be $\tau_s=37$ MPa [4]. Keeping all other parameters the same ($h=\frac{1}{20}$, $\rho=8$, and $\rho_{olap}=50\%$), the stiffness of the wet nacre is estimated to be 64.80 GPa, whereas the tensile strength is estimated to be 147 MPa (the plateau is approximately at 140 MPa). These results are in excellent agreement with the experimentally determined values of 60 GPa and 140 MPa for the stiffness and tensile strength, respectively [4]. Figure 12 presents a comparison of the stress-strain response for dry and wet nacre assuming a maximum shear strain of $\epsilon_{max}=20\%$ in the organic matrix. Since the effect of water is to increase the ductility (maximum shear strain, ϵ_{max}) of the organic matrix, based on the results presented in Fig. 10, it can be concluded that the work of fracture of wet nacre is greater than that of dry nacre.

E. Strength of aragonite platelets

So far, we have assumed that tension elements representing the aragonite mineral platelets do not fail. This is indeed consistent with the experimenal observations [4], wherein the failure of platelets is not detected. However, in order to design synthetic nanocomposites with fracture properties

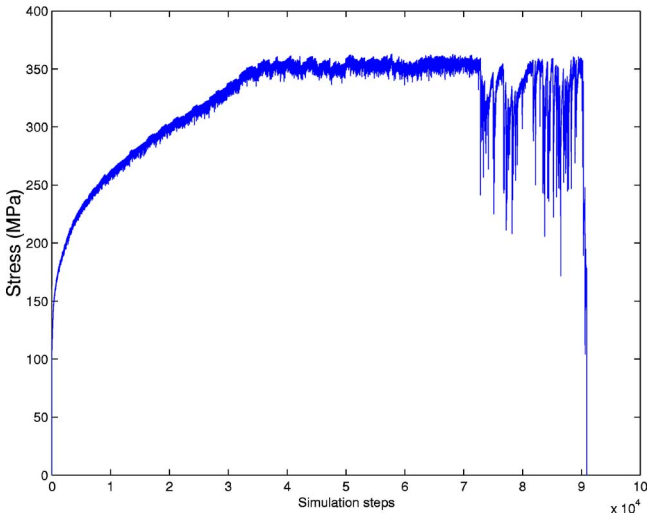

FIG. 13. (Color online) Maximum tensite stress in any of the aragonite platelets during a typical simulation.

comparable to those of nacre, it is necessary to understand the levels of stress that are sustained by these hard mineral platelets. In the synthesis of nanocomposites, knowing these stress levels will enable us to select appropriate hard mineral materials that mimic the functionality of aragonite platelets.

Since the aragonite platelets are divided into ρ number of tension elements, the tensile stresses in these platelets build up from the ends of the platelet and attain maximum at the center of the platelets. During various numerical simulations with perfect and random BM architecture, we have observed that the maximum tensile stresses in the aragonite platelets varied between 350–400 MPa. Figure 13 presents the maximum tensile stress observed in any of the aragonite platelet elements during a typical simulation. For a platelet aspect ratio of $\rho=8$ and the mean shear strength $\tau_s=46$ MPa of the organic matrix, the mineral strength based on Griffith criterion [23] results in 368 MPa, which is consistent with the result presented in Fig. 13. Hence, in order to design synthetic composites with fracture properties comparable to that of nacre, it becomes necessary for the mineral platelets to sustain tensile stresses of the order of 400 MPa. It should however be noted that these computed maximum tensile stresses in the aragonite platelets are an order of magnitude smaller than the theoretical strength, σ_{th}, of a perfect aragonite crystal ($\sigma_{\text{th}} \approx E_p/30 \approx 3$ GPa).

IV. CONCLUSIONS

This study presented a simple continuous damage random thresholds fuse network model to understand the fracture behavior of nacre. The significance of the proposed numerical model is that it captures the essential physics of the problem; namely the underlying "brick and mortar" architecture and the modular damage evolution of the organic interface between the aragonite platelets. The discrete fuse lattice topology mimics the nacre's unique BM microarchitecture such that the aragonite platelets are modeled by fuses that never fail and the organic matrix between the aragonite platelets is modeled by shear elements (fuses) that can fail multiple times thereby representing the modular damage evolution that is characteristic of organic polymers. Indeed, multiple failures of shear elements (fuses) in the CDRFM results in a modular sawtoothlike force-extension behavior that is consistent with the force-extension behavior of a fiber bundle of mineral bridges between the aragonite platelets and the force-extension curves corresponding to a repeated unfolding of protein molecules in the organic polymer adhesive. It is in this sense that the multiple failures of fuses in the CDRFM represent the effect of mineral bridges and the organic polymer adhesive. Compared with the previous analytical and numerical models, the significance of the proposed CDRFM model is that it is the first model that can accurately capture the plateau (ductility) of the nacre's stress-strain response, the onset of yielding, and the work of fracture, which was not possible with the previously existing models.

The numerical results obtained using this simple CDRFM are in excellent agreement with the previously obtained experimental results, the stiffness of (dry) nacre is estimated to be 73.61 GPa as against experimentally determined value of 70 GPa; the stress-strain response exhibited a plateau with a tensile strength of 175 MPa as against experimentally determined value of 167 MPa; and the results clearly indicate that the work of fracture of nacre is significantly (orders of magnitude) larger than that of pure aragonite mineral. For wet nacre, the estimated stiffness is 64.80 GPa compared to an experimental value of 60 GPa, and the stress-strain response is similar to that of dry nacre response, which exhibited a plateau corresponding to a tensile strength of 140 MPa that is in excellent agreement with the experimental tensile strength of 140 MPa. Assuming that the effect of water is to increase the ductility of the organic matrix, the results presented in Fig. 10 suggest that the work of fracture of wet nacre is significantly higher than that of dry nacre.

To summarize, nacre's phenomenal fracture behavior is due to three important factors: namely, the perfect BM arrangement of platelets with maximum overlap area between platelets, the mean shear strength of the organic matrix, and the modular damage evolution aspect of the organic matrix that can withstand very large strains before complete interface failure occurs. In particular, its superior toughness is a direct consequence of ductility (maximum shear strain) of the organic matrix, and its high fracture strength is a result of its unique BM architecture with significant overlap of the platelets, and the shear strength of the organic matrix.

Based on our computational modeling studies, in order to artificially synthesize tough ceramics or nanoscale biocomposites, it is necessary that the constituent materials possess the following properties:

(i) Mimic the nacres unique BM arrangement of mineral platelets and organic matrix with significant overlap of the platelets.

(ii) The damage in the organic matrix evolves in a modular fashion corresponding to the sawtoothlike force-extension behavior. In addition, the ductility (maximum shear strain at which the ultimate failure of the organic matrix occurs) of the organic matrix should be large.

(iii) The tensile strength of the mineral platelets should exceed 400 MPa.

ACKNOWLEDGMENTS

This research is sponsored by the Mathematical, Information and Computational Sciences Division, Office of Advanced Scientific Computing Research, U.S. Department of Energy under Contract No. DE-AC05-00OR22725 with UT-Battelle, LLC. One of the authors (P.K.V.V.N.) thanks Dr. Surya Ganti for his valuable suggestions.

[1] J. D. Currey, Proc. R. Soc. London, Ser. B **196**, 443 (1977).
[2] A. P. Jackson, J. F. V. Vincent, D. Briggs, R. A. Crick, S. F. Davies, M. J. Hearn, and R. M. Turner, J. Mater. Sci. Lett. **5**, 975 (1986).
[3] A. P. Jackson, J. F. V. Vincent, and R. M. Turner, Proc. R. Soc. London, Ser. B **234**, 415 (1988).
[4] A. P. Jackson, J. F. V. Vincent, and R. M. Turner, J. Mater. Sci. **25**, 3173 (1990).
[5] M. Sarikaya, J. Liu, and I. A. Aksay, Biomimetics: design and processing of materials, New York, 1995, pp. 35–90.
[6] G. Mayer and M. Sarikaya, Exp. Mech. **42**, 395 (2002).
[7] R. Z. Wang, H. B. Wen, F. Z. Cui, H. B. Zhang, and H. D. Li, J. Mater. Sci. **30**, 2299 (1995).
[8] B. L. Smith, T. E. Schaffer, M. Viani, J. B. Thompson, N. A. Frederick, J. Kindt, A. Belcher, G. D. Stucky, D. E. Morse, and P. K. Hansma, Nature (London) **399**, 761 (1999).
[9] S. Kamat, X. Su, R. Ballarini, and A. H. Heuer, Nature (London) **405**, 1036 (2000).
[10] A. G. Evans, Z. Suo, R. Z. Wang, I. A. Aksay, M. Y. He, and J. W. Hutchinson, J. Mater. Res. **16**, 2475 (2001).
[11] R. Z. Wang, Z. Suo, A. G. Evans, N. Yao, and I. A. Aksay, J. Mater. Res. **16**, 2485 (2001).
[12] K. Okumura and P.-G. de Gennes, Eur. Phys. J. E **4**, 121 (2001).
[13] R. Menig, M. H. Meyers, M. A. Meyers, and K. S. Vecchio, Mater. Sci. Eng., A **297**, 203 (2001).
[14] J. F. V. Vincent, Philos. Trans. R. Soc. London, Ser. B **358**, 1597 (2003).
[15] N. Almqvist, N. H. Thomson, B. L. Smith, G. D. Stucky, D. E. Morse, and P. K. Hansma, Mater. Sci. Eng., C **7**, 37 (1999).
[16] K. Okumura, Europhys. Lett. **67**, 470 (2004).
[17] T. E. Schaffer, C. I-Zanetti, R. Proksch, M. Fritz, D. A. Walters, N. Almqvist, C. M. Zaremba, A. M. Belcher, B. L. Smith, G. D. Stucky, D. E. Morse, and P. K. Hansma, Chem. Mater. **9**, 1731 (1997).
[18] F. Song and Y. L. Bai, J. Mater. Res. **18**, 1741 (2003).
[19] F. Song, A. K. Soh, and Y. L. Bai, Biomaterials **24**, 3623 (2003).
[20] I. Jager and P. Fratzl, Biophys. J. **79**, 1737 (2000).
[21] S. P. Kotha, Y. Li, and N. Guzelsu, J. Mater. Sci. **36**, 2001 (2001).
[22] D. R. Katti, K. S. Katti, J. M. Sopp, and M. Sarikaya, Comput. Theor. Polym. Sci. **11**, 397 (2001).
[23] H. Gao, B. Ji, I. L. Jager, E. Arzt, and P. Fratzl, Proc. Natl. Acad. Sci. U.S.A. **100**, 5597 (2003).
[24] B. Ji and H. Gao, Mater. Sci. Eng., A **366**, 96 (2004).
[25] L. de Arcangelis, S. Redner, and H. J. Herrmann, J. Phys. (Paris), Lett. **46**, 585 (1985); M. Sahimi and J. D. Goddard, Phys. Rev. B **33**, 7848 (1986).
[26] L. de Arcangelis, A. Hansen, H. J. Herrmann, and S. Roux, Phys. Rev. B **40**, 877 (1989).
[27] *Statistical Models for the Fracture of Disordered Media*, edited by H. J. Herrmann and S. Roux (North-Holland, Amsterdam, 1990); *Non-Linearity and Breakdown in Soft Condensed Matter*, edited by K. K. Bardhan, B. K. Chakrabarti, and A. Hansen (Springer-Verlag, Berlin, 1994); B. K. Chakrabarti and L. G. Benguigui, *Statistical Physics of Fracture and Breakdown in Disordered Systems* (Oxford University Press, Oxford, 1997); D. Krajcinovic and J. G. M. van Mier, *Damage and Fracture of Disordered Materials* (Springer-Verlag, New York, 2000).
[28] S. Zapperi, P. Ray, H. E. Stanley, and A. Vespignani, Phys. Rev. Lett. **78**, 1408 (1997); Phys. Rev. E **59**, 5049 (1999).
[29] S. Zapperi, A. Vespignani, and H. E. Stanley, Nature (London) **388**, 658 (1997).
[30] F. Kun, S. Zapperi, and H. J. Herrmann, Eur. Phys. J. B **17**, 269 (2000).
[31] R. C. Hidalgo, F. Kun, and H. J. Herrmann, Phys. Rev. E **64**, 066122 (2001).
[32] D. Amitrano, J. R. Grasso, and D. Hantz, Geophys. Res. Lett. **26**, 2109 (1999).
[33] P. K. V. V. Nukala and S. Simunovic, J. Phys. A: Math. Gen. **36**, 11403 (2003).
[34] G. G. Batrouni and A. Hansen, Phys. Rev. Lett. **80**, 325 (1998).